Selective and Fast Detection of Fluoride-Contaminated Water Based on a Novel Salen-Co-MOF Chemosensor

Maha Alhaddad and Said M. El-Sheikh*

ACCESS | Metrics & More | Article Recommendations | SI Supporting Information

ABSTRACT: The development of selective and fast optical sensitive chemosensors for the detection and recognition of different cations and anions in a domain is still a challenge in biological, industrial, and environmental fields. Herein, we report a novel approach for the detection and determination of fluoride ion (F^-) sensing based on a salen-cobalt metal-organic framework (Co(II)-MOF). By a simple method, the Co(II)-MOF was synthesized and characterized using several tools to elucidate the structure and morphology. The photoluminescence (PL) spectrum of the Co(II)-MOF (100.0 nM/L) was examined versus different ionic species like F^-, Br^-, Cl^-, I^-, SO_4^{2-}, and NO_3^- and some cationic species like Mg^{2+}, Ca^{2+}, Na^+, and K^+. In the case of F^- ions, the PL intensity of the Co(II)-MOF was scientifically enhanced with a remarkable red shift. With the increase of F^- concentration, the Co(II)-MOF PL emission spectrum was also professionally enhanced. The limit of detection (LOD) for the Co(II)-MOF chemosensor was 0.24 μg/L, while the limit of quantification (LOQ) was 0.72 μg/L. Moreover, a comparison of the Co(II)-MOF optical approach with other published reports was studied, and the mechanism of interaction was also investigated. Additionally, the applicability of the current Co(II)-MOF approach in different real water samples, such as tap water, drinking water, Nile River water, and wastewater, was extended. This easy-to-use future sensor provides reliable detection of F^- in everyday applications for nonexpert users, especially in remote rural areas.
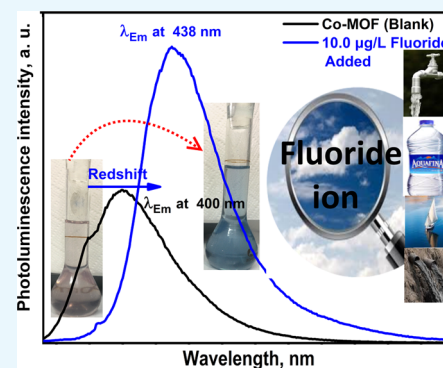
INTRODUCTION

Nowadays, the rapid growth of industries and population worldwide has increased the demand for clean water everywhere and therefore become a vital area of research, attracting the interest of all scientists in this field.[1−3] In addition, the limited availability of new water resources makes the treatment process of wastewater and its reuse essential and sustainable. It is well known that there are different types of organic and inorganic pollutants in water sources such as dyes, solvents, heavy metals, etc. All of these pollutants should be treated before using the water by humans, animals, etc.[4] Most of the industries generate a certain amount of wastewater containing different pollutants, and one of the largest pollutants in streams is the fluoride ion (F^-) from the separation of uranium process, fertilizers, processing of metals, manufacturing of glass, etc.[1,3,5] Besides the industrial sources, F^- is present in many natural sources, and in groundwater, it is one of the most abundant anions due to the dissolution process of fluoride-rich rocks as fluorapatite, villiaumite, fluorspar, and cryolite.[6−8]

F ions, one of the excellent micronutrients, are used in many fields, for example, dental physicians use them as a toothpaste additive to inhibit dental cavities and increase teeth resistance to acid corrosion by the effect of bacteria, and they are also valuable to bone growth.[9,10] Additionally, they are used in many countries as an additive in drinking water and tap water

and also in the treatment process, but lately used under supervision.[1,11,12]

In spite of the numerous vital applications of F ions, like any cation or anion, the increasing or decreasing F ion ingestion or intake by humans could cause many detrimental effects even at small concentration levels; it can cause a lot of diseases, such as minamata, acrodynia, renal failure, nervous disorder, immune system dysfunction, dangerous impairment to the brain, heart, stomach, and liver.[1,11] So, some international organizations like "The American Dental Association (ADA) and The U.S. Environmental Protection Agency (EPA)" recommended F^- concentrations of ∼0.6 to 1.2 mg/L and ∼2 to 4 mg/L in bottled water and drinking water, respectively.[9,13] A F^- dose of 1.5−4.0 mg/day is recommended in an adult diet, and for children in their first 12 months, the dietary recommended dose per day is 0.1−1 mg.[1,4] In a recent study,[14] the statistical results showed that about 200 million people, in about 25 countries, are still under the danger of F^- overdoses.[15−17]
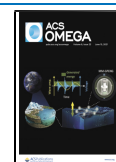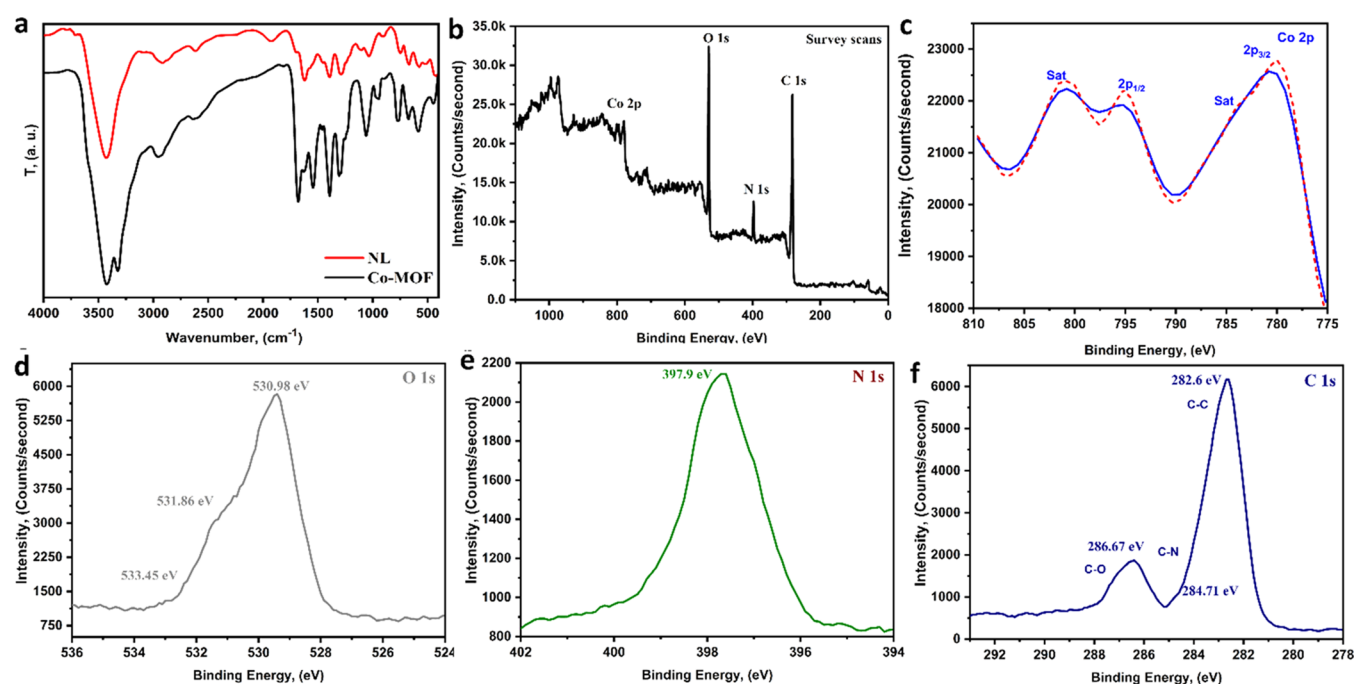
Figure 1. (a) FT-IR spectra of the nanolinker (NL) and the Co(II)-MOF. (b)−(f) XPS analysis of the cobalt metal−organic framework (Co(II)-MOF): (b) survey, (c) Co 2p, (d) O 1s, (e) N 1s, and (f) C 1s.

Therefore, the removal and/or detection of fluoride ions in ground- and wastewater has always been of concern.[2,18] Additionally, efficient, applicable, and low-cost technologies of water treatment and detection are required.[19,20] Many analytical methodologies and techniques have been used for the detection of F^{−}, such as inductively coupled plasma optical spectrometry,[11] ^{19}F-NMR,[1,21] ion-selective electrodes,[22] ion chromatography,[23] atomic absorption spectrometry (AAS), gas chromatography-mass spectrometry (GC−MS),[24] etc.[25] However, some of the above approaches need complicated and expensive instrumentation, procedures, and/or long-term analysis. On the other hand, fluorescent sensors, especially based on metal−organic frameworks (MOFs), have offered many advantages and unique properties of high sensitivity, superselectivity, lower detection, and quantification limits and can also be used for anion live cell imaging.[7,21,26−30]

MOFs are a family of organic−inorganic hybrid structures, which are formed via coordination bonding between functionalized linkers and the center of metal ions, have many unique properties, and are used in a huge number of vital applications.[31−43]

Recently, the development and exploration of fluoride ions, luminescent chemical sensors, and removal based on MOFs have become enormously significant. For example, for F^{−} detection, Sharafizadeh et al. prepared urea-based MOFs and used them as promising chemical sensors for F^{−} and H_2AsO_4 anions in groundwater pollutants.[2] Xie et al. reported an NH_2-MIL-53(Al) MOF for the simultaneous F^{−} detection and removal method; its detection limit (LOD) was 0.31 μmol/L with a wide response of 0.5−100 μmol/L.[3] Wang et al. reported that Y(III)-based rare-earth-MOF nanoplates were used for the detection of pH and F^{−} in two water resources (natural and pH in real water) with a LOD of 8.5 ppb.[4] Sun et al. demonstrated a chemiluminescence approach for F^{−} detection using a hybrid MOF based on NH_2-MIL-101(Al) with a linear response of 0.5−80.0 μmol/L and a LOD of 0.05

μmol/L.[7] Zhu et al. examined the adsorption behavior of MOF-801 for F^{−}, and the adsorption capacity was 40 mg/g F^{−} at 30 °C; the prepared MOF was used successively for the efficient removal of F^{−} from water.[8] Zeng et al. reported a visual method using smartphones based on mixed La-MOFs in a linear range of 0−1.9 ppm with a LOD of 96 ppb.[9] Wentz et al. synthesized a redox-active naphthalene diimide-MOF and it showed a reversible and selective color-change response to F^{−}.[1212] Zhu et al. mentioned that the luminescence of NH_2-UiO-66 can be used for F^{−} detection in water medium with a LOD of 0.229 mg/L.[21] Zhao et al. showed the incorporation of fluorescent molecules in a zirconium-based (UiO-66)-MOF for F^{−} detection in aqueous solutions with a LOD of 4.4×10^{-3} mM.[27] Mantasha et al. prepared a porous Cu(II)-MOF and used it as a F^{−} sensor with a LOD of 1.203 ppb.[44] Hinterholzinger et al. reported a selective and sensitive method based on the release of fluorophores from the NH_2-MIL-101(Al)-MOF.[45] Wan et al. synthesized a luminescent porous three-dimensional (3D) Tb-MOF and used it for the F^{−} detection in aqueous solution.[46] Wang et al. revealed that a luminescent Eu(III)-MOF can be used as a turn-on efficient fluorescent sensor for F^{−}, PO_4^{3-}, and Fe^{3+} detection with the naked eye under UV irradiation.[47]

In this work, a novel Co(II)-MOF was synthesized for the first time and characterized using several tools such as high-resolution transmission electron microscopy (HR-TEM), field emission scanning electron microscopy/energy-dispersive X-ray (FE-SEM/EDX), CHN elemental analysis, Fourier transform infrared spectroscopy (FT-IR), mass spectrometry, thermogravimetry/differential scanning calorimetry (TG/DSC), ultraviolet−visible (UV−vis) spectroscopy, X-ray photoelectron spectroscopy (XPS), X-ray diffraction (XRD), and magnetic properties. The prepared Co(II)-MOF was used as a promising chemosensor for F^{−}. The nature of the sensing mechanism was established based on Lewis acid−base and an open cobalt center, which offer recognition of specific small

molecules like F^- even in the presence of other competing cationic or anionic species. The results of the present study indicated that the Co(II)-MOF may be used as a chemosensor with promising merits for the F^- detection at ultralow concentration levels with statically satisfactory results. Moreover, a comparison of the Co(II)-MOF PL optical method with other available published studies besides the mechanism of interactions was investigated. The current Co(II)-MOF PL optical method collects all of the figures of merit of the previous reports, for example, it exemplifies lower quantification and detection limits, extensive reproducibility, significant selectivity and sensitivity, simplicity of the preparation/operation technologies, and extra selectivity.

■ RESULTS AND DISCUSSION

Co(II)-MOF Characterization. The Co(II)-MOF was synthesized according to the reaction given in Scheme S1 in the Supporting Information. A violet precipitate of the Co(II)-MOF was characterized using several tools. The structure interpretation and elucidation based on physicochemical analysis were investigated in detail.

Elemental Analysis. The elemental analysis (C/H/N) of the synthesized Co(II)-MOF was carried out. The analysis data were in great agreement with the theoretically estimated one for the assumed monomeric Co(II)-MOF unit formula. The analysis calculation (%) was $C_{48}H_{85}Co_2N_9O_{27}$ (1338.11 g/mol); C, 43.09; H, 6.40; N, 9.42; found (%) C, 43.09; H, 6.39; N, 9.90, and the melting point (mp) was >300 °C. Additionally, the reaction yield of Co(II)-MOF was 65.7%.

Mass Spectrum. The mass spectrum of the synthesized Co(II)-MOF and assumed schematic mass fragmentations are presented in Figure S1 and Scheme S2 in the Supporting Information, respectively. From Figure S1, it can be noticed that m/z bands were absolutely harmonized with the assumed formula practically from the above obtained elemental data. The theoretical peak of the molecular ion estimated at $1338.11m/z$ in the mass spectrum was shifted to $900m/z$. Afterward, the sequential fragmentations as presented in Scheme S2 were in satisfactory agreement with the suggested structure molecular weight of $C_{48}H_{85}Co_2N_9O_{27}$. The ion at $m/z = 1338.11$ under mass fragmentations successively showed a steady peak at $m/z = 801.59$ (the theoretical peak was calculated at $m/z = 801.50$) with the absence of 3 ethanol, 14 water, and 2 dimethylformamide (DMF) molecules. Afterward, the compound showed additional decomposition, leading to mass fragmentations at $\sim m/z = 638, 475, 165, 108, 107, 93, 74, 66,$ and 59. Generally, the succeeding mass fragmentations of the Co(II)-MOF were completely consistent with the values computed theoretically and the molecular weight suggested for the structure.

FT-IR Spectra. The FT-IR spectrum was recorded for the comparison of the Co(II)-MOF and the NL spectrum, and the results are shown in Figure 1a. For the Co(II)-MOF, the peaks in the range of 3697−3074 cm^{-1} were assigned to H_2O and NH_2 molecules. The band centered at 3426 cm^{-1}, which was assigned to $\nu(OH)$, broadly evidenced the presence of a large amount of water and the intra/inter Co-MOF site structure.[48] The bands centered at around 2562 cm^{-1} were attributed to C−C≡O carbonyl bonds. The bands between 1769 and 1530 cm^{-1} and positioned at 1640 cm^{-1} were attributed to the stretching/bending of $\nu(C=O)/\nu(NH)$. The band at 1380 cm^{-1} was assigned to the stretching vibration of C−O.[48] The peaks between 1058 and 765 cm^{-1} were attributed to aromatic

benzene $\nu(CH)$.[49] The bands appearing at 582 and 441 cm^{-1} were attributed to the coordinate and covalent bonding of the cobalt ion with O and N ($\nu(Co < -O)$ and $\nu(Co-N)$), respectively.[48] The existence of these two new fangled bands established and proved the complexation/chelation of the cobalt ion throughout the oxygen and nitrogen atoms of NL.[50,51]

UV−Vis Band Gap Energy Spectra. The comparison of UV−vis/NIR band gap energy (BGE) spectra of the NL and the Co(II)-MOF is shown in Figure S2 in the Supporting Information. Figure S2a−c represents the UV−vis/NIR spectra at different scales arranged between 2000 and 200 nm; it was noticed that the Co(II)-MOF show a sharp band at 234 nm and three bands at 351, 415, and 630 nm. Furthermore, Figure S2d shows the BGE of the linker and the Co(II)-MOF. It was noticed that the BGE of the linker was at 3.64, 2.96, 2.0 eV, and in the case of Co(II)-MOF, it reduced to 3.24, 2.48, and 1.98 eV, respectively. The decrease in BGE was due to high linker conjugation, which caused an increase in the HOMO valence band energy; therefore, the BGE of the Co(II)-MOF decreased.[52,53]

XRD Pattern. The Co(II)-MOF PXRD pattern in comparison with the published reports is displayed in Figure S3 in the Supporting Information.[54,55] The spectrum revealed that no sharp peaks were present for the rest of the Co(II)-MOF bands, suggesting that the amorphous phase was achieved. From the Co(II)-MOF XRD spectrum compared with the published Co(II)-MOF spectra,[50,56,57] it can be noted that the peaks belonging to Co-MOF-74 were at 7.0, 9.35, 16.25, 18.11, 29.11, 31.13, 33.32, and 45.88°.[56] It was also noted that the threadbare Co-MOF harmonized well with the two-dimensional (2D) Co-MOF simulated pattern.[50,57] Additionally, more details of the XRD data, including the values of the lattice parameter, interplanar distances, Miller indices, and particle size of Co(II)-MOF that were calculated using the Scherrer equation, are presented in Tables S1 in the Supporting Information.

XPS Analysis. The XPS spectra of the prepared Co(II)-MOF sample are shown in Figure 1b−f. The Co(II)-MOF survey scans (Figure 1b) revealed the sample contents of Co, C, O, and N as construction element blocks free of impurities. The XPS peak of Co 2p (Figure 1c) revealed signals ascribed to Co(II) $2p_{1/2}$ and $2p_{3/2}$, which confirmed the presence of Co(II) in the MOF.[58] The XPS O 1s peaks (Figure 1d) displayed three peaks for O−Co−O at 530.98 eV, C−O at 531.86 eV, and C=O at 533.45 eV. The XPS N 1s peak (Figure 1e) showed a single peak at 397.9 eV for quaternary N. The C 1s XPS spectrum (Figure 1f) showed the presence of three signals at 282.60 eV for C−C, 284.71 eV for C−N, and 286.67 eV for C=O.

Thermal Analysis. The thermal behavior of Co(II)-MOF was investigated by TGA/DSC plots (Figure S4 in the Supporting Information). The plots suggested that the Co(II)-MOF go through four collapse phases. In the first phase, a weight loss of about 26.21% was due to the loss of ethanol and intrastructure water molecules at temperatures starting from 68 to 172.43 °C (theoretically calculated weight loss was 26.48%). In the second phase, a weight loss of about 13.69% was due to the loss of DMF and interstructure water molecules at temperatures up to 350.54 °C (theoretically calculated weight loss was 13.62%). The third collapse phase was due to the exclusion of organic ligands at a starting temperature of 355.8 °C with a weight loss of about 51.15%. In
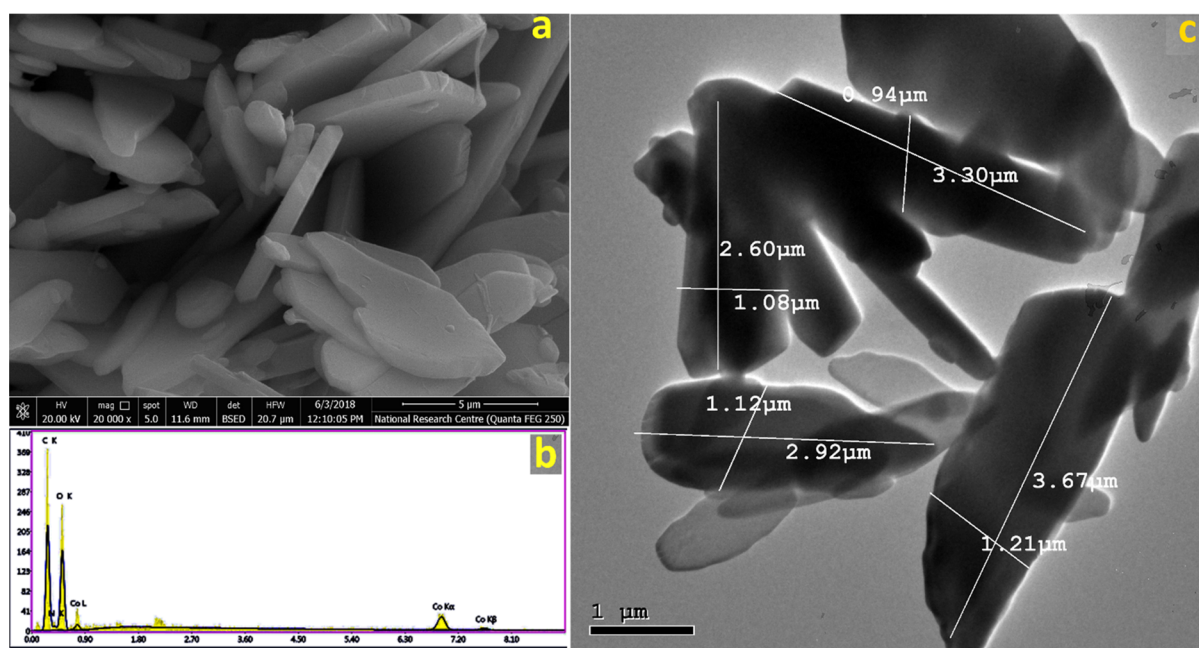
Figure 2. (a) Field emission scanning electron microscopy image of the cobalt metal−organic framework (Co(II)-MOF), (b) energy-dispersive X-ray analysis with the single-point EDX mapping analysis of Co(II)-MOF, and (c) the transmission electron microscopy image (TEM) of the Co(II)-MOF.
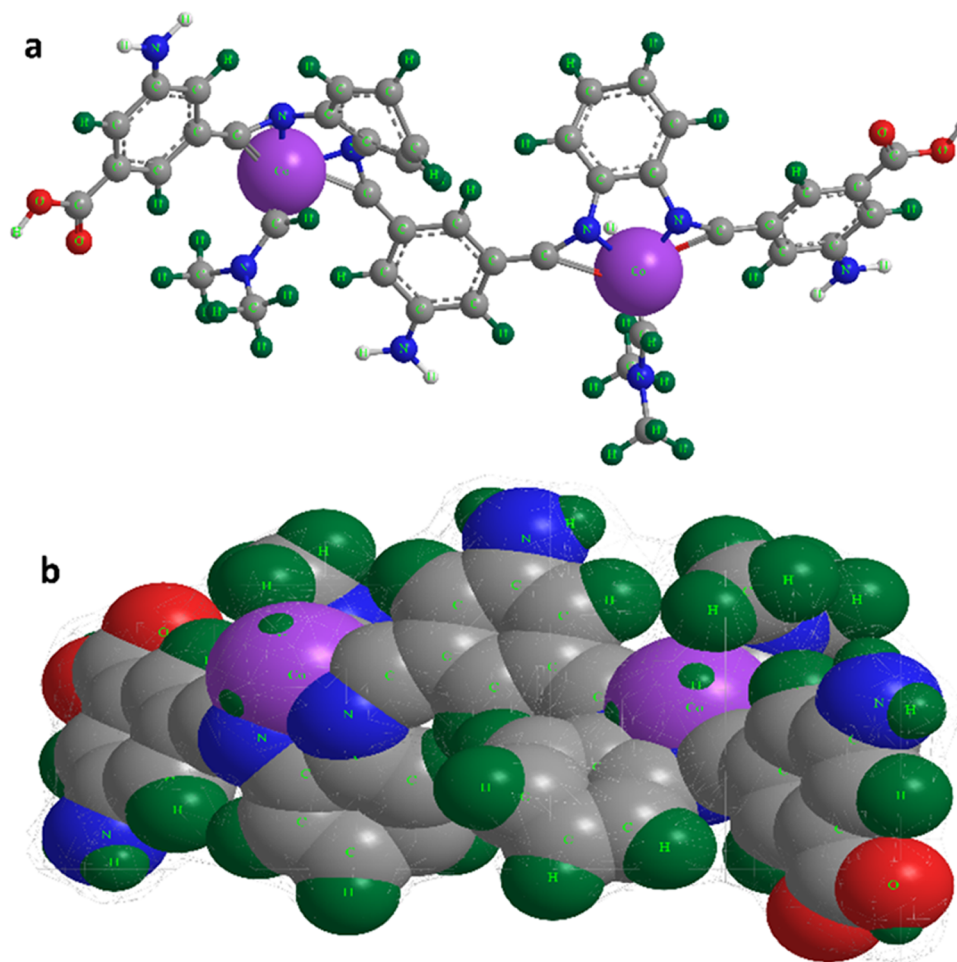
Figure 3. (a) 3D structural representation of the Co(II)-MOF monomeric unit and (b) advanced molecular surface representation of the Co(II)-MOF monomeric unit.
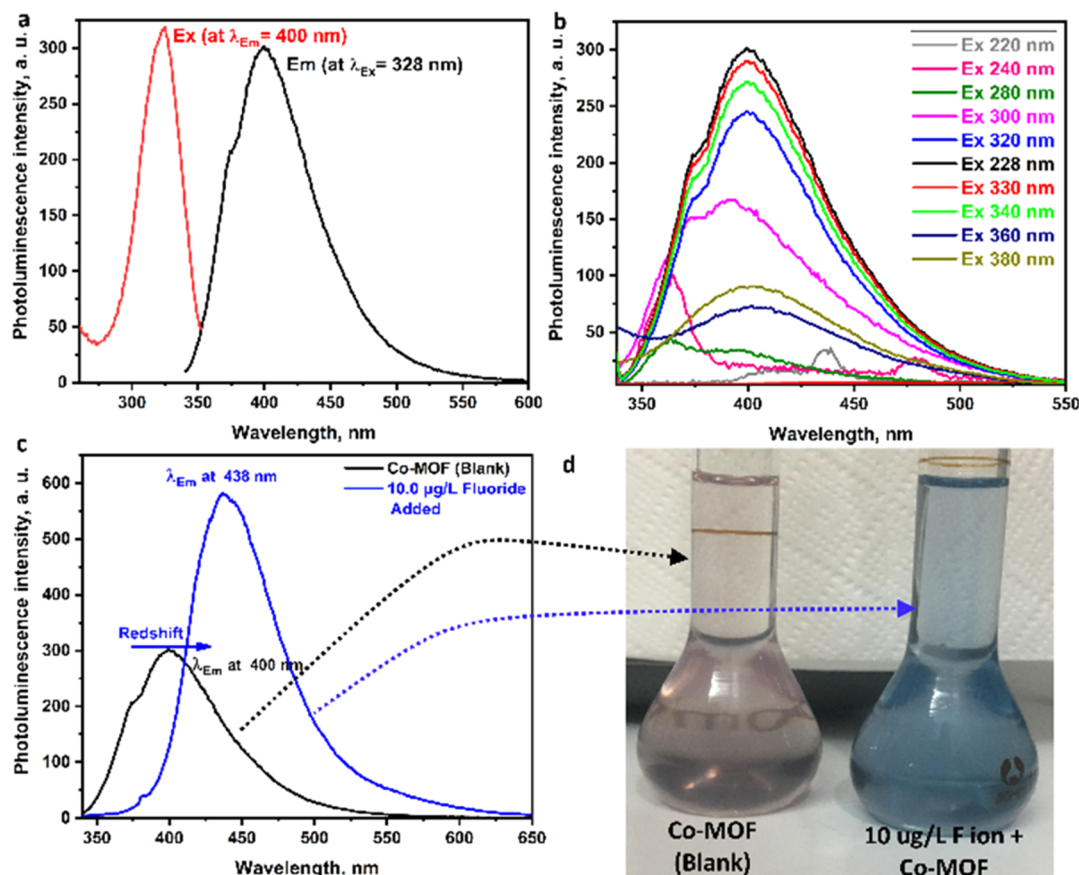
Figure 4. (a) Excitation (red line) and emission (black line) spectra of the Co(II)-MOF, (b) PL emission spectra at different excitation wavelengths for the Co(II)-MOF, (c) the photoluminescence spectra response for the behavior of the Co(II)-MOF against 10.0 μg/L F$^-$, and (d) a smartphone photography image for providing the sensing activity of the Co(II)-MOF against 10.0 μg/L F$^-$.

the last phase, the remaining residue of Co was 8.95%. The above data supported the mass and mass fragmentation data as well as the data obtained from the XRD and CHN analyses.[59]

FE-SEM and TEM Spectroscopy. The Co(II)-MOF FE-SEM, EDX, and TEM images are displayed in Figure 2. The morphology of the Co(II)-MOF based on the viewed FE-SEM image (Figure 2a) appeared to be 2D Co-MOF nanowalls, aligned in an orderly manner.[50] The nanowalls displayed a smooth surface with an average thickness of around 450 nm, estimated from the enlarged side view.[50] Furthermore, the EDX mapping analysis (Figure 2b and Table S2 in the Supporting Information) of the Co(II)-MOF showed the presence of cobalt, carbon, oxygen, and nitrogen as construction element blocks in the nanowalls. The outstanding dispersion of the above MOF elements alongside the cross section revealed by EDX mapping analysis (Figure 2b) also confirmed the Co(II)-MOF construction. Moreover, as shown in Table S2, the reported EDX results were in agreement with those theoretically computed as well as with elemental CHN analysis data: C, 43.09; Co, 8.81; N, 9.42; and O, 32.28; found: C, 43.09; Co, 8.72; N, 9.90; and O, 38.29. The TEM image of the Co(II)-MOF appeared like uniform 2D nanowalls with an aspect ratio of 3, as shown in Figure 2c.

Co(II)-MOF Magnetic Behavior. The magnetization curvature of the Co(II)-MOF (Figure S5 in the Supporting Information) showed a saturated magnetization value (Ms) of about 18.308 emu/g with a coercivity of 11.995 G and a remanence of 0.13320 emu/g. From the magnetization curvature, it can be noticed that the superparamagnetic

behavior of the Co(II)-MOF was due to the smallest crystallite size compared with massive noninteracting magnetic moments.[60]

From the above obtained physical/spectral data, we can presume the 3D Co(II)-MOF monomeric unit structure and its molecular advanced surface as presented in Figure 3a,b, respectively.

Photoluminescence (PL) Study and Application. The photoluminescence (PL) spectrum of the Co(II)-MOF was investigated. At room temperature, the emission\excitation spectra were achieved using autosurvey mode in an excitation wavelength range of 220−550 nm at a scanning rate interval of 20 nm and an emission wavelength range of 240−900 nm at a slide width of 5 nm. Under optimized conditions, it was observed that the Co(II)-MOF (Figure 4a) displayed an emission peak at 400 nm after excitation at 328 nm. Also, the PL spectra of the Co(II)-MOF were manually investigated at distinctive excitation wavelengths, and emission peaks were recorded as represented in Figure 4b. The Co(II)-MOF fluorescent behavior can be ascribed to the $\pi-n$ and $\pi-\pi^*$ molecular orbital transitions (MOTs) in the ligand/ligand−metal charge transfer (LMCT).[61−63] Additionally, the Co(II)-MOF was studied as a spectrofluorimetric chemosensor for F$^-$ detection.

The PL spectrum (at λ_{ex} = 328 nm) of the Co(II)-MOF (0.1 μM/L) was investigated against 10.0 μg/L F$^-$ (Figure 4c). As shown in Figure 4c, the intensity of the PL spectrum of the Co(II)-MOF was remarkably enhanced with a significant red shift from 400 to 438 nm. Additionally, as shown from the
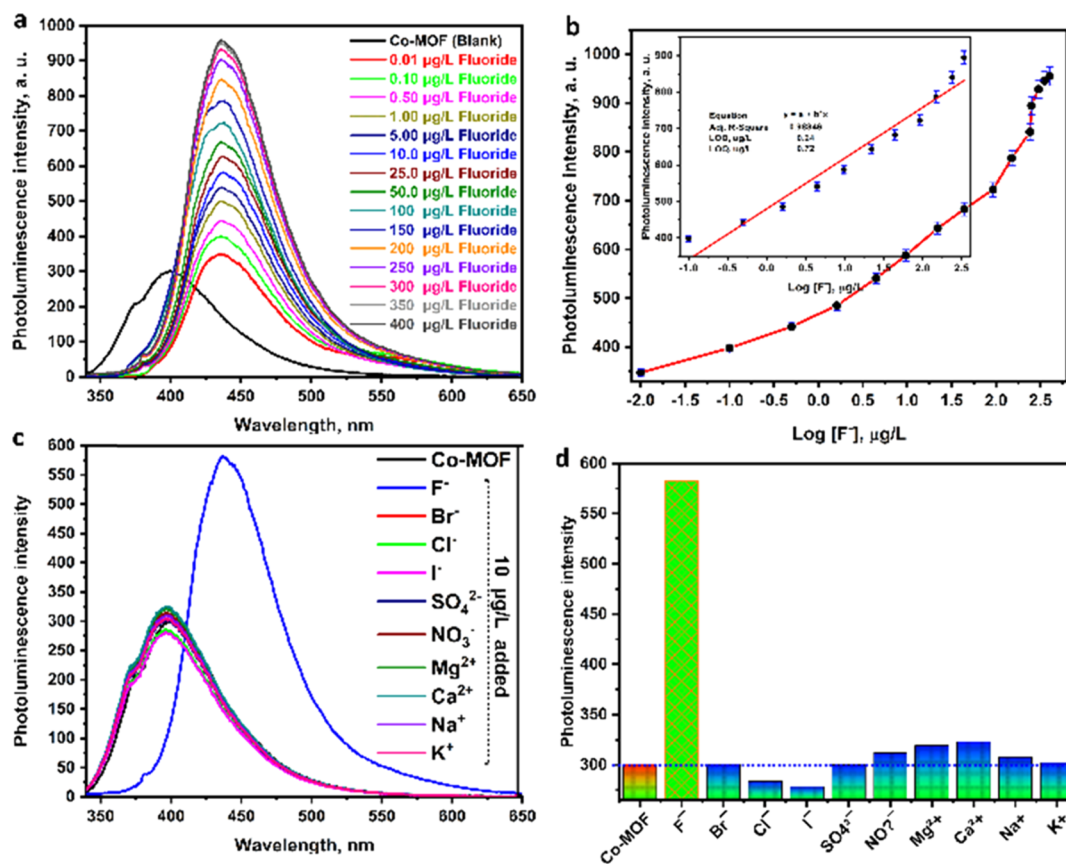
Figure 5. (a) Photoluminescence spectra response for the behavior of the Co(II)-MOF toward different concentrations of F^-. (b) A calibration graph between the photoluminescence intensity of the Co(II)-MOF and the logarithm of fluorine ion concentrations ($\log[F^-]$). The inset shows a linear dynamic concentration range of the calibration graph. (c) The photoluminescence intensity of the Co(II)-MOF toward F^- against different types of interfering analytes. (d) A histogram of the photoluminescence intensity spectrum of the Co(II)-MOF toward F^- against different types of interfering analytes.

smartphone photography image (Figure 4d), the solution color of the Co(II)-MOF transformed from violet to blue, which makes the Co(II)-MOF an applicable naked-eye indicator for F^-. Besides, the PL spectrum of the Co(II)-MOF versus different concentrations of F^- was examined, and the obtained record data is shown in Figure 5a. As shown in the above figures, the Co(II)-MOF intensities of the PL spectrum were remarkably enhanced with a significant peak red shift of peaks from λ_{400} to λ_{438}, after excitation at λ_{328}, as the optimal concentration increased from 0.01 to 400 μg/L, with contrast in colors from violet to blue. The above results demonstrated that the Co(II)-MOF could be used as a fast optical fluorometric chemosensor for F^- quantification and detection.

Method Validation and Analytical Performance for F^- Detection. *Calibration Curve, Quantification, and Detection Limits.* Under optimal conditions, the standard calibration curve between Co(II)-MOF PL intensities at λ_{ex} = 328 nm versus F^- concentrations (in a range from 0.01 to 400 μg/L) is presented in Figure 5b. It was noticed from Figure 5b that the PL spectrum intensities were substantially dependent on the increase of the F^- concentration and that PL λ_{438} increased and subsequently reached a saturation point at a F^- concentration of 400 μg/L. The standard calibration curve showed a linear fit correlation over the range of 0.1−339.0 μg/L (the inset of Figure 5b) and the tailoring equation is expressed as follows

$$PL\ intensity = 479.65 + 139.02\ [F^-]$$

with $r^2 = 0.988$ \hfill (1)

The LOD for the Co(II)-MOF chemosensor was 0.24 μg/L, while the LOQ was 0.72 μg/L. The summarized regression data analysis for PL intensity is represented in Table 1. A wide linear concentration range and lower LOD\LOQ values confirm the prominent sensitivity of the proposed Co(II)-MOF chemosensor. Likewise, the comparison of LOD and the working linear concentration range values for the detection of

Table 1. Sensitivity and Regression Parameters for the Co(II)-MOF Chemosensor

parameter	method
λ_{ex} (nm)	328
λ_{em} (nm)	438
linear range (μg/L)	0.1−388
limit of detection (LOD) (μg/L)	0.24
limit of quantification (LOQ) (μg/L)	0.72
regression equation	$(Y = a + bX)^a$
intercept (a)	479.65
slope (b)	139.02
standard deviation	10.22
correlation coefficient (r^2)	0.95

^{a}Y, photoluminescence intensities; X, the concentration of F^- in μg/L; a, intercept; and b, slope.

F⁻ based on different MOFs in previously published articles[3,4,7,9,21,27,28,46] and our present approach is briefed in Table 2.

Table 2. Comparison between the Co(II)-MOF Chemosensor and Some Published Methods for the Determination of F⁻

method	linear range	LOD (μg/L)	refs
NH2-MIL-53(Al)-MOF	9.5−189.9 μg/L	5.89	3
Y(III)-based rare-earth-MOF nanoplates	0.05−8.0 mg/L	8.5	4
luminescent NH2-MIL-101(Al)-MOF-based chemiluminescence approach	9.5 μg/L−1.52 mg/L	0.95	7
La-MOFs based on the visual method	0−1.9 mg/L	96.0	9
luminescent NH2-UiO-66-MOF	0−50 mg/L	229.0	21
zirconium-based (UiO-66)-MOF	0−7.6 mg/L	83.59	27
luminescence colorimetric (1) and fluorescence (2) dual modes		2.07 (1) 7.43 (2)	28
luminescent porous 3D Tb-MOF		9.44	46
Co(II)-MOF chemosensor	0.1−388 μg/L	0.24	this work

Accuracy, Precision, Reducibility, and Repeatability. In the present study, a typical statistical assessment is conducted to recognize the applicability and efficacy of the assumed optical fluorometric approach based on the Co(II)-MOF to quantitate and detect F⁻. The present work was carried out at five concentrations (0.1, 1.0, 10.0, 100, and 250 μg/L); each test was repeated three times on "the same and different days (repeatability and reproducibility study)". The results of the PL intensities of the Co(II)-MOF against different concentrations of F⁻ are summarized in Table S3 in the Supporting Information. From the analysis of the obtained table data, the average percentages of relative error values "RE %" evaluated were ~1.0 and 0.98% for intra- and interday, respectively; which indicates the extraordinary accuracy, repeatability, and reducibility of the implied approach. The estimated mean "X" values were very near to true values; the standard deviation "SD" values were ~1.0 and 2.19, whereas the coefficient of variation "CV" values were 3.25 and 3.06 for intra- and interday, respectively. The estimated lower values of RE %, SD, and CV revealed the precision, repeatability, and reducibility of the proposed approach.

Selectivity. The Co(II)-MOF PL behavior toward F⁻ ions and different anions and cations as interfering varieties based on the suggested PL optical fluorometric approach was examined to demonstrate the identifiable selectivity and to prove the ability for F⁻ ions recognition. The PL spectrum of the Co(II)-MOF (0.1 μM/L) was studied against 10 μg/L of some ionic species like F⁻, Br⁻, Cl⁻, I⁻, SO_4^{2-}, and NO_3^- and some cationic species like Mg^{2+}, Ca^{2+}, Na^+, and K^+. The results of the selectivity study, PL spectrum, and enhancement efficiency histogram are represented in Figure 5c,d. As shown in Figure 5c,d, in the case of F⁻ ions, the PL intensities were scientifically enhanced with a remarkable red shift, and did not give any obvious responses for any interfering species. So, we can deduce that the Co(II)-MOF is exceptionally

selective for F⁻ ions throughout the remarkable red shift with the enhancement effect.

Recovery Study and Real Sample Applications. The current assumed approach was explored to quantize the F⁻ concentration in different water samples. F⁻ was spiked in the water samples at five concentrations (0.1, 1.0, 10.0, 100, and 250 μg/L), and after repeating the three trials of the assay, the summary of the obtained results is reported in Table S4 in the Supporting Information. The statistical assessments of the gained data were done by the calculation of "recovery (RC%) and relative standard deviation (RSD%)". The summarized data reveal that the RC values were between 98.15 and 101.4% with RSD % between 0.01 and 3.42 for tap water samples, 96.7 and 102% with RSD % between 0.01 and 5.33 for bottled water samples, 91.49 and 101.2% with RSD % between 0.03 and 4.65 for river water samples, and 94.66 and 103.5% with RSD % between 0.03 and 3.39 for wastewater samples. Subsequently, the average recovery percentages were 99.46, 98.47, 97.13, and 97.34% for tap, bottled, river, and wastewater samples, respectively. The present data demonstrate that the optical fluorometric approach could be applicable and effective for the detection of F⁻ in diverse water samples and future promising analytical tools interested in F⁻ quantification.

Mechanism of Interaction. Typically, the Co(II)-MOF exhibited violet emission photoluminescence at 400 nm after excitation at 328 nm. Upon the formation of the Co(II)-MOF-F⁻ sensing platform, a distinctive fast host−guest response was noticed between F⁻ and the Co(II)-MOF, resulting in a red shift from 400 to 438 nm with remarkable photoluminescence enhancement (Figures 4c and 5a). Additionally, by visual detection, the photoluminescence color obviously transformed from violet to blue after the interaction, which was easily noticed with the naked eye (Figure 4d). The above interactions provided the exceptional photoluminescence response for F⁻ and were explored due to the following: First, F⁻ detection based on fluorescent chemosensors may depend on the deprotonation of CH, NH, OH, etc., moieties[1,64] and hydrogen bonding[65] to change their optical behavior or due to the affinity or reactivity of F⁻ toward Lewis acids. Second, the Co-MOF structure had 2, 4, and 6 coordination numbers, which provided a large number of coordinated cobalt metal centers with d-orbitals, part of them were used for coordination with ligands, whereas the redundant open metal site provided the binding or adsorption positions and high probability of replacement toward F⁻.[4,9] Third, the fluorine ion has the smallest ion radius among all varieties of anions, which makes F⁻ the easiest replacement of solvents like H_2O in the Co-MOF unit cell, enhancing the frequency of the interaction between F⁻ and the Co-MOF.[4,9] Fourth, a Lewis acid−base strong interaction may occur between the Co-MOF and F⁻, such as Lewis acid−base and open metal centers, offering specific recognition of small molecules such as F⁻.[4] Lastly, the strong electronegativity of the fluoride ion made a photoinduced electron transfer within the Co-MOF structure, leading to a photoluminescence red shift.[66−68] The resulting exclusive host−guest interactions (Lewis acid−base interactions) between the host site (Co-MOF) and the guest site (F⁻) induced a fast photoluminescence behavior with the Co-MOF, and finally, a highly sensitive, selective, and applicable fluoride ion chemosensor was developed.

■ CONCLUSIONS

Promising cobalt (II) metal−organic framework nanowalls were synthesized via a facile route for the first time and confirmed via several characterizations. CHN, mass spectra, and EDX mapping analysis data were in agreement with the theoretically calculated values for the assumed formula of the Co(II)-MOF monomeric unit. Other characterization data such as FT-IR, UV−vis band gap energy spectra, XRD, and XPS were in good agreement with the proposed structure. Thermal analysis supported the mass and mass fragmentations data as well as the data obtained from the XRD and CHN analyses.

The obtained Co-MOF was used for the detection of F^-. The PL spectrum intensity of the Co(II)-MOF was remarkably enhanced with a significant red shift from 400 to 438 nm. Additionally, the color of the Co(II)-MOF solution transforms from violet to blue, which makes the Co(II)-MOF an applicable naked-eye indicator for F^-. The study of the PL results showed that the Co-MOF can be used as a fast, selective, and sensitive optical chemosensor for F^- detection in the presence of different interfering cations and anions based on a comparison with the other published reports. The sensitivity of the proposed Co(II)-MOF chemosensor was also confirmed by a wide linear concentration range and lower LOD\LOQ values. The average percentages of relative error values RE % evaluated were ~1.0 and 0.98% for intra- and interday, respectively, which indicates the extraordinary accuracy, repeatability, and reducibility of the suggested approach.

The mechanism of interaction was investigated, and the resulting exclusive host/guest interactions (Lewis acid/base interactions) between the Co(II)-MOF (as the host site) and F^- (as the guest site) induced a fast photoluminescence behavior with the Co-MOF with highly sensitive and selectivity. The present data demonstrate that the assumed optical fluorometric approach could be applicable and effective for F^- detection in diverse water samples and future promising analytical tools interested in F^- quantification.

■ EXPERIMENTAL SECTION

Materials. See the details in the Supporting Information.

Instruments. See the details in the Supporting Information.

Synthesis Procedure of the Co(II)-MOF. The Co(II)-MOF was synthesized based on a nanolinker (NL) prepared according to ref 69. In this manner, $CoCl_2 \cdot 6H_2O$ (0.4759 g, 2.0 mmol) was added gradually into a flask containing the NL. The mixture was refluxed for two days when the color of the solution turned from a light brown suspension to a violet precipitate. The formed Co(II)-MOF was filtered off, washed several times, and dried at 90 °C for 24 h.

General Procedure of PL Measurements. A stock solution (1.0 μM/L) of the Co(II)-MOF was prepared by dissolving it in DMSO and then diluted with distilled H_2O. Subsequently, the diluted stock solution of Co(II)-MOF (100.0 nM/L) was subjected to consequent PL measurements. The PL intensities of the Co(II)-MOF (100.0 nM/L) solution were recorded against different concentrations of the F^- solution and other different analytes.

Determination of F^- Ions Using the Co(II)-MOF. The PL spectrum of the Co(II)-MOF (0.1 μM/L) against the above prepared different concentrations of F^- was detected.

Under optimized conditions of PL measurements, a linear correlation was accomplished between the PL intensities of the Co(II)-MOF at an excitation wavelength of λ_{ex} = 328 nm and F^- concentrations in a range between 0.01 and 400 μg/L.

Additionally, the LOD and LOQ were estimated from eqs 2 and 3[70−72]

$$LOD = (3.3 \times S)/b \tag{2}$$

$$LOD = (10.0 \times S)/b \tag{3}$$

where S is the value of the standard error of PL intensities and b is the linear graph slope of the curve of calibration.

Quantification of F^- Ions in Different Real Samples. The real water samples were obtained from different resources (the sample of tap water was from our laboratory, bottled drinking water was bought from a local supermarket, the river water sample was from Egypt Nile River, and wastewater sample was from waste canals), subjected to primary filtration, and centrifuged at 4000 rpm for 10 min.

■ ASSOCIATED CONTENT

ⓢ Supporting Information

The Supporting Information is available free of charge at https://pubs.acs.org/doi/10.1021/acsomega.1c01424.

> Proposed mechanism of Co(II)-MOF synthesis; proposed fragmentation scheme; mass spectrum; electronic reflection spectra; band gap energy; X-ray diffraction spectra; thermogravimetric analysis; magnetization curve; summary of XRD data; EDX analysis; evaluation of intraday and interday accuracy, precision study; and determination of F^- in different real samples (PDF)

■ AUTHOR INFORMATION

Corresponding Author

Said M. El-Sheikh − *Nanomaterials and Nanotechnology Department, Central Metallurgical R & D Institute, Cairo 11421, Egypt;* ⓘ orcid.org/0000-0002-2570-8326; Phone: +20 1022316076; Email: selsheikh2001@gmail.com

Author

Maha Alhaddad − *Department of Chemistry, Faculty of Science, King Abdulaziz University, Jeddah 21589, Kingdom of Saudi Arabia*

Complete contact information is available at:
https://pubs.acs.org/10.1021/acsomega.1c01424

Author Contributions

The research was conceived and the experiments were performed by S.M.E.-S. The two authors contributed to data analyses and writing the manuscript.

Notes

The authors declare no competing financial interest.

■ ACKNOWLEDGMENTS

■ REFERENCES

(1) Dhiman, S.; Ahmad, M.; Singla, N.; Kumar, G.; Singh, P.; Luxami, V.; Kaur, N.; Kumar, S. Chemodosimeters for Optical Detection of Fluoride Anion. *Coord. Chem. Rev.* **2020**, *405*, No. 213138.

(2) Sharafizadeh, M.; Mokhtari, J.; Saeidian, H.; Mirjafary, Z. Anion Recognition by Urea Metal−Organic Frameworks: Remarkable Sensitivity for Arsenate and Fluoride Ions. *Environ. Sci. Pollut. Res.* **2020**, *27*, 25132−25139.

(3) Xie, D.; Ge, X.; Qin, W.; Zhang, Y. NH 2 -MIL-53 (Al) for Simultaneous Removal and Detection of Fluoride anions. *Chin. J. Chem. Phys.* **2020**, *34*, 227−237.

(4) Wang, X.; Chu, C.; Wu, Y.; Deng, Y.; Zhou, J.; Yang, M.; Zhang, S.; Huo, D.; Hou, C. Synthesis of Yttrium (III) -Based Rare-Earth Metal-Organic Framework Nanoplates and Its Applications for Sensing of Fl Uoride Ions and PH. *Sens. Actuators, B* **2020**, *321*, No. 128455.

(5) Gavrilescu, M.; Pavel, L. V.; Cretescu, I. Characterization and Remediation of Soils Contaminated with Uranium. *J. Hazard. Mater.* **2009**, *163*, 475−510.

(6) Jagtap, S.; Yenkie, M. K.; Labhsetwar, N.; Rayalu, S. Fluoride in Drinking Water and Defluoridation of Water. *Chem. Rev.* **2012**, *112*, 2454−2466.

(7) Sun, Y.; Xu, X.; Zhao, Y.; Tan, H.; Li, Y.; Du, J. Luminescent Metal Organic Frameworks−Based Chemiluminescence Resonance Energy Transfer Platform for Turn−on Detection of Fluoride Ion. *Talanta* **2020**, *209*, No. 120582.

(8) Zhu, X.-H.; Yang, C. X.; Yan, X. P. Metal-Organic Framework-801 for Efficient Removal of Fluoride from Water. *Microporous Mesoporous Mater.* **2018**, *259*, 163−170.

(9) Zeng, X.; Hu, J.; Zhang, M.; Wang, F.; Wu, L.; Hou, X. Visual Detection of Fluoride Anions Using Mixed Lanthanide Metal-Organic Frameworks with a Smartphone. *Anal. Chem.* **2020**, *92*, 2097−2102.

(10) Everett, E. T. Critical Reviews in Oral Biology & Medecine: Fluoride's Effects on the Formation of Teeth and Bones, and the Influence of Genetics. *J. Dent. Res.* **2011**, *90*, 552−560.

(11) Maung, P.; Beauchemin, D. Development of a Method for the Direct Determination of Fluorine in Solid Samples Using Electrothermal Vaporization Coupled to Inductively Coupled Plasma Optical Emission Spectrometry. *J. Anal. At. Spectrom.* **2020**, *35*, 1097−1102.

(12) Wentz, H. C.; Campbell, M. G. Fluoride Detection with a Redox-Active Naphthalene Diimide Metal−Organic Framework. *Polyhedron* **2018**, *154*, 309−313.

(13) Hu, R.; Feng, J.; Hu, D.; Wang, S.; Li, S.; Li, Y.; Yang, G. A Rapid Aqueous Fluoride Ion Sensor with Dual Output Modes. *Angew. Chem. Int. Ed.* **2010**, *49*, 4915−4918.

(14) Ayoob, S.; Gupta, A. K. Fluoride in Drinking Water: A Review on the Status and Stress Effects. *Crit. Rev. Environ. Sci. Technol.* **2006**, *36*, 433−487.

(15) Mondal, P.; Anweshan, A.; Purkait, M. K. Chemosphere Green Synthesis and Environmental Application of Iron-Based Nanomaterials and Nanocomposite: A Review. *Chemosphere* **2020**, *259*, No. 127509.

(16) Haldar, D.; Duarah, P.; Purkait, M. K. MOFs for the Treatment of Arsenic, Fl Uoride and Iron Contaminated Drinking Water: A Review. *Chemosphere* **2020**, *251*, No. 126388.

(17) Mondal, P.; Purkait, M. K. Green Synthesized Iron Nanoparticles Supported on PH Responsive Polymeric Membrane for Nitrobenzene Reduction and Fl Uoride Rejection Study: Optimization Approach. *J. Clean. Prod.* **2018**, *170*, 1111−1123.

(18) Mohapatra, M.; Anand, S.; Mishra, B. K.; Giles, D. E.; Singh, P. Review of Fluoride Removal from Drinking Water. *J. Environ. Manage.* **2009**, *91*, 67−77.

(19) Zhou, Y.; Zhang, J. F.; Yoon, J. Fluorescence and Colorimetric Chemosensors for Fluoride-Ion Detection. *Chem. Rev.* **2014**, *114*, 5511−5571.

(20) Beer, P. D.; Gale, P. A. Anion Recognition and Sensing: The State of the Art and Future Perspectives. *Angew. Chem. Int. Ed.* **2001**, *40*, 486−516.

(21) Zhu, H.; Huang, J.; Zhou, Q.; Lv, Z.; Li, C.; Hu, G. Enhanced Luminescence of NH2-UiO-66 for Selectively Sensing Fluoride Anion in Water Medium. *J. Lumin.* **2019**, *208*, 67−74.

(22) Buffle, J.; Parthasarathy, N.; Haerdi, W. Study of the Behaviour of Solid-State Membrane Electrodes: Part II. Role of Adsorption of Fluoride Ions on Fluoride Ion-Selective Electrode and Determination of Solubility of the Membrane. *Anal. Chim. Acta* **1974**, *68*, 253−266.

(23) Breadmore, M. C.; Palmer, A. S.; Curran, M.; Macka, M.; Avdalovic, N.; Haddad, P. R. On-Column Ion-Exchange Preconcentration of Inorganic Anions in Open Tubular Capillary Electrochromatography with Elution Using Transient-Isotachophoretic Gradients. 3. Implementation and Method Development. *Anal. Chem.* **2002**, *74*, 2112−2118.

(24) Pagliano, E.; Meija, J.; Ding, J.; Sturgeon, R. E.; D'ulivo, A.; Mester, Z. Novel Ethyl-Derivatization Approach for the Determination of Fluoride by Headspace Gas Chromatography/Mass Spectrometry. *Anal. Chem.* **2013**, *85*, 877−881.

(25) Yahyavi, H.; Kaykhaii, M.; Mirmoghaddam, M. Recent Developments in Methods of Analysis for Fluoride Determination. *Crit. Rev. Anal. Chem.* **2016**, *46*, 106−121.

(26) He, J.; Xu, J.; Yin, J.; Li, N.; Bu, X. H. Recent Advances in Luminescent Metal-Organic Frameworks for Chemical Sensors. *Sci. China Mater.* **2019**, *62*, 1655−1678.

(27) Zhao, X.; Wang, Y.; Hao, X.; Liu, W. Fluorescent Molecule Incorporated Metal-Organic Framework for Fluoride Sensing in Aqueous Solution. *Appl. Surf. Sci.* **2017**, *402*, 129−135.

(28) Chen, P.; Zhu, H.; Kong, L.; Xu, X.; Tian, Y.; Yang, J. Multifunctional Behavior of a Novel Tetraphenylethylene Derivative: Mechanochromic Luminescence, Detection of Fluoride Ions and Trace Water in Aprotic Solvents. *Dye. Pigment.* **2020**, *172*, No. 107832.

(29) Ebrahim, F. M.; Nguyen, T. N.; Shyshkanov, S.; Gladysiak, A.; Favre, P.; Zacharia, A.; Itskos, G.; Dyson, P. J.; Stylianou, K. C. Selective, Fast-Response, and Regenerable Metal-Organic Framework for Sampling Excess Fluoride Levels in Drinking Water. *J. Am. Chem. Soc.* **2019**, *141*, 3052−3058.

(30) Chen, B.; Wang, L.; Zapata, F.; Qian, G.; Lobkovsky, E. B. A Luminescent Microporous Metal - Organic Framework for the Recognition. *J. Am. Chem. Soc.* **2008**, *130*, 6718−6719.

(31) Alhaddad, M.; Sheta, S. M. Dual Naked-Eye and Optical Chemosensor for Morphine Detection in Biological Real Samples Based on Cr(III) Metal−Organic Framework Nanoparticles. *ACS Omega* **2020**, *5*, 28296−28304.

(32) Sheta, S. M.; El-Sheikh, S. M.; Abd-Elzaher, M. M. Simple Synthesis of Novel Copper Metal−Organic Framework Nanoparticles: Biosensing and Biological Applications. *Dalton Trans.* **2018**, *47*, 4847−4855.

(33) Sheta, S. M.; El-sheikh, S. M.; Osman, D. I.; Salem, A. M.; Ali, O. I.; Harraz, F. A.; Shousha, W. G.; Shoeib, M. A.; Shawky, S. M.; Dionysiou, D. D. A Novel HCV Electrochemical Biosensor Based on a Polyaniline@Ni-MOF Nanocomposite. *Dalton Trans.* **2020**, *49*, 8918−8926.

(34) Sheta, S. M.; El-Sheikh, S. M.; Abd-Elzaher, M. M.; Wassel, A. R. A Novel Nano - Size Lanthanum Metal − Organic Framework Based on 5 - Amino - Isophthalic Acid and Phenylenediamine: Photoluminescence Study and Sensing Applications. *Appl. Organometal Chem.* **2019**, *33*, No. e4777.

(35) Kökçam-Demir, Ü.; Gharib, M.; Morsali, A.; Weingart, O.; Janiak, C.; Goldman, A. Coordinatively unsaturated metal sites (open metal sites) in metal−organic frameworks: design and applications. *Chem. Soc. Rev.* **2020**, 2751−2798.

(36) Sheta, S. M.; El-Sheikh, S. M.; Abd-Elzaher, M. M. Promising Photoluminescence Optical Approach for Triiodothyronine Hormone Determination Based on Smart Copper Metal − Organic Framework Nanoparticles. *Appl. Organometal Chem.* **2019**, *33*, No. e5069.

(37) Liang, J.; Nuhnen, A.; Millan, S.; Breitzke, H.; Gvilava, V.; Buntkowsky, G.; Janiak, C. Encapsulation of a Porous Organic Cage into the Pores of a Metal − Organic Framework for Enhanced CO 2 Separation. *Angew. Chem. Int. Ed.* **2020**, *59*, 6068−6073.

(38) Gruber, I.; Nuhnen, A.; Lerch, A.; Nießing, S.; Klopotowski, M.; Herbst, A.; Karg, M.; Janiak, C. Synthesis of Nano / Microsized MIL-101Cr Through Combination of Microwave Heating and Emulsion Technology for Mixed-Matrix Membranes. *Front. Chem.* **2019**, *7*, No. 777.

(39) Sheta, S. M.; El-sheikh, S. M.; Abd-elzaher, M. M. A Novel Optical Approach for Determination of Prolactin Based on Pr-MOF Nanofibers. *Anal. Bioanal. Chem.* **2019**, *411*, 1339−1349.

(40) Sheta, S. M.; El-Sheikh, S. M.; Abd-Elzaher, M. M.; Salem, S. R.; Moussa, H. A.; Mohamed, R. M.; Mkhalid, I. A. A Novel Biosensor for Early Diagnosis of Liver Cancer Cases Using Smart Nano-Magnetic Metal − Organic Framework. *Appl. Organometal Chem.* **2019**, *33*, No. e5249.

(41) Osman, D. I.; El-sheikh, S. M.; Sheta, S. M.; Ali, O. I.; Salem, A. M.; Gh, W.; El-khamisy, S. F.; Shawky, S. M. Biosensors and Bioelectronics Nucleic Acids Biosensors Based on Metal-Organic Framework (MOF): Paving the Way to Clinical Laboratory Diagnosis. *Biosens. Bioelectron.* **2019**, *141*, No. 111451.

(42) Basaleh, A. S.; Sheta, S. M. Novel Advanced Nanomaterial Based on Ferrous Metal − Organic Framework and Its Application as Chemosensors for Mercury in Environmental and Biological Samples. *Anal. Bioanal. Chem.* **2020**, *412*, 3153−3165.

(43) Basaleh, A. S.; Sheta, S. M. Manganese Metal−Organic Framework: Chemical Stability, Photoluminescence Studies, and Biosensing Application. *J. Inorg. Organomet. Polym. Mater.* **2021**, *31*, 1726−1737.

(44) Mantasha, I.; Shahid, M.; Saleh, H. A. M.; Qasem, K. M. A.; Musheer, A. A Novel Sustainable Metal Organic Framework as the Ultimate Aqueous Phase Sensor for Natural Hazards: Detection of Nitrobenzene and F−at the Ppb Level and Rapid and Selective Adsorption of Methylene Blue. *CrystEngComm* **2020**, *22*, 3891−3909.

(45) Hinterholzinger, F. M.; Rühle, B.; Wuttke, S.; Karaghiosoff, K.; Bein, T. Highly Sensitive and Selective Fluoride Detection in Water through Fluorophore Release from a Metal-Organic Framework. *Sci. Rep.* **2013**, *3*, No. 2562.

(46) Wan, Y.; Sun, W.; Liu, J.; Liu, Z. A 3D Porous Luminescent Terbium Metal-Organic Framework for Selective Sensing of F− in Aqueous Solution. *Inorg. Chem. Commun.* **2017**, *80*, 53−57.

(47) Wang, Q.-S.; Li, J. J.; Zhang, M. N.; Li, X. A Luminescent Eu(III)-Based Metal-Organic Framework as a Highly Effective Sensor for Cation and Anion Detections. *Sens. Actuators, B* **2018**, *258*, 358−364.

(48) Wu, Y.; Song, X.; Li, S.; Yang, X.; Shen, P.; Gao, L.; Wei, R.; Zhang, J.; Xiao, G.; et al. 3D-Monoclinic M−BTC MOF (M = Mn, Co, Ni) as Highly Efficient Catalysts for Chemical Fixation of CO2 into Cyclic Carbonates. *J. Ind. Eng. Chem.* **2018**, *58*, 296−303.

(49) Yin, D.; Li, C.; Ren, H.; Shekhah, O.; Liu, J.; Liang, C. Efficient Pd@MIL-101(Cr) Hetero-Catalysts for 2-Butyne-1,4-Diol Hydrogenation Exhibiting High Selectivity. *RSC Adv.* **2017**, *7*, 1626−1633.

(50) Tao, K.; Han, X.; Mab, Q.; Han, L. A Metal−Organic Framework Derived Hierarchical Nickel−Cobalt Sulfide Nanosheet Array on Ni Foam with Enhanced Electrochemical Performance for Supercapacitors. *Dalton Trans.* **2018**, *47*, 3496−3502.

(51) Mokhles, M.; Abd-Elzaher, Said M.; El-shiekh; Eweis, M. Biological Studies of Newly Synthesized Ferrocenyl Complexes Containing Triazinone Moiety. *Appl. Organomet. Chem.* **2006**, *20*, 798−810.

(52) El-sheikh, S. M.; Rabbah, M. Novel Low Temperature Synthesis of Spinel Nano-Magnesium Chromites from Secondary Resources. *Thermochim. Acta* **2013**, *568*, 13−19.

(53) Ahmed, Y. M. Z.; El-Sheikh, S. M.; Zaki, Z. I. Changes in Hydroxyapatite Powder Properties via Heat Treatment. *Bull. Mater. Sci.* **2015**, *38*, 1807−1819.

(54) Liu, X.; Cheng, S.; Long, J.; Zhang, W.; Liu, X.; Wei, D. MOFs-Derived Co@CN Bi-Functional Catalysts for Selective Transfer Hydrogenation of *α,β*-Unsaturated Aldehydes without Use of Base Additives. *Mater. Chem. Front.* **2017**, *1*, 2005−2012.

(55) Ramachandran, R.; Rajavel, K.; Xuan, W.; Lin, D.; Wang, F. Influence of Ti3C2Tx (MXene) Intercalation Pseudocapacitance on

Electrochemical Performance of Co-MOF Binder-Free Electrode. *Ceram. Int.* **2018**, *44*, 14425−14431.

(56) Sun, J.; Zhang, X.; Zhang, A.; Liao, C. Preparation of Fe − Co Based MOF-74 and Its Effective Adsorption of Arsenic from Aqueous Solution. *J. Environ. Sci.* **2018**, *80*, 197−207.

(57) Zhang, J.; Zhang, T.; Yu, D.; Xiao, K.; Hong, Y. Transition from ZIF-L-Co to ZIF-67: A New Insight into the Structural Evolution of Zeolitic. *CrystEngComm* **2015**, *17*, 8212−8215.

(58) Cheng, J.; Chen, S.; Chen, D.; Dong, L.; Wang, J.; Zhang, T.; Jiao, T.; Liu, B.; Wang, H.; Kai, J.; et al. Editable Asymmetric All-Solid-State Supercapacitors Reduced Graphene Oxide Self-Assembled Papers. *J. Mater. Chem. A* **2018**, *6*, 20254−20266.

(59) Kim, K.; Lopez, K. J.; Sun, H.-J.; An, J.-C.; Park, G.; Shim, J. Electrochemical Performance of Bifunctional Co / Graphitic Carbon Catalysts Prepared from Metal − Organic Frameworks for Oxygen Reduction and Evolution Reactions in Alkaline Solution. *J. Appl. Electrochem.* **2018**, *48*, 1231−1241.

(60) El-shiekh, S. M.; Abd-Elzaher, M. M.; Eweis, M. Synthesis, Characterization and Biocidal Studies of New Ferrocenyl Thiadiazolo-Triazinone Complexes. *Appl. Organomet. Chem.* **2006**, *20*, 505−511.

(61) Pickwick, B. L.; Pochodylo, A. L.; LaDuca, R. L. Luminescent Cadmium Coordination Polymers Synthesized from Bis(4-Pyridylmethyl)Piperazine and Isophthalic Acid Derivatives. *Inorg. Chim. Acta* **2017**, *458*, 146−162.

(62) Han, M.; Chang, X.; Feng, X.; Ma, L.; Wang, L. Temperature and PH Driven Self-Assembly of Zn(II) Coordination Polymers: Crystal Structures, Supramolecular Isomerism, and Photoluminescence. *CrystEngComm* **2014**, *16*, 1687−1695.

(63) Allendorf, M. D.; Bauer, C. A.; Bhakta, R. K.; Houk, R. J. T. Luminescent Metal−Organic Frameworks. *Chem. Soc. Rev.* **2009**, *38*, 1330−1352.

(64) Li, Z.; Huang, N.; Lee, K. H.; Feng, Y.; Tao, S.; Jiang, Q.; Nagao, Y.; Irle, S.; Jiang, D. Light-Emitting Covalent Organic Frameworks: Fluorescence Improving via Pinpoint Surgery and Selective Switch-On Sensing of Anions. *J. Am. Chem. Soc.* **2018**, *140*, 12374−12377.

(65) Uttam, B.; Kandi, R.; Hussain, M. A.; Rao, C. P. Fluorescent Lower Rim 1,3-Dibenzooxadiazole Conjugate of Calix[4]Arene in Selective Sensing of Fluoride in Solution and in Biological Cells Using Confocal Microscopy. *J. Org. Chem.* **2018**, *83*, 11850−11859.

(66) Zhang, L.; Wang, J.; Du, T.; Zhang, W.; Zhu, W.; Yang, C.; Yue, T.; Sun, J.; Li, T.; Wang, J. NH2- MIL-53 (Al) Metal − Organic Framework as the Smart Platform for Simultaneous High-Performance Detection and Removal of Hg 2+. *Inorg. Chem.* **2019**, *58*, 12573−12581.

(67) Pal, S.; Bhunia, A.; Jana, P. P.; Dey, S.; Möllmer, J.; Janiak, C.; Nayek, H. P. Microporous La-Metal-Organic Framework (MOF) with Large Surface Area. *Chem. - Eur. J.* **2015**, *21*, 2789−2792.

(68) Wu, Y.; Wu, W.; Zou, L.; Feng, J.; Gu, C.; Li, B.; Batten, S. R.; Yadav, R.; Kumar, A. Luminescent Sensing of a New 8-Connected Topological Metal-Organic Framework. *Inorg. Chem. Commun.* **2016**, *70*, 160−163.

(69) Sheta, S. M.; El-Sheikh, S. M.; Abd-Elzaher, M. M.; Ghanemc, M. L.; Salem, S. R. A Novel, Fast, High Sensitivity Biosensor for Supporting Therapeutic Decisions and Onset Actions for Chest Pain Cases †. *RSC Adv.* **2019**, *9*, 20463−20471.

(70) Abd-Elzaher, M. M.; Ahmed, M. A.; Farag, A. B.; Attia, M. S.; Youssef, A. O.; Sheta, S. M. A Fast and Simple Method for Determination of Testosterone Hormone in Biological Fluids Based on a New Eu(III) Complex Optical Sensor. *Sens. Lett.* **2017**, *15*, 977−981.

(71) Abd-Elzaher, M. M.; Ahmed, M. A.; Farag, A. B.; Attia, M. S.; Youssef, A. O.; Sheta, S. M. New Optical Sensor for Determination of Hydrochlorothiazide in Pharmaceutical Preparation and Biological Fluids. *Sens. Lett.* **2017**, *15*, 525−530.

(72) Abd-Elzaher, M. M.; Ahmed, M. A.; Farag, A. B.; Attia, M.; Youssef, A. O.; Sheta, S. M. Characterization of Eu(III) Complex for Determination of Bumetanide in Pharmaceutical Preparations and in Biological Fluids. *Egypt. J. Chem.* **2016**, *59*, 701−718.